Combustion Synthesis and Luminescent Properties of Red-Emitting $Sr_{4-x}Al_6MoO_{16}$:xEu^{3+} Phosphors

B. V. Tupte[*1], M. M. Bhave[2], C. D. Mungmode[3], D. H. Gahane[2], S. V. Moharil[4]

[*1]Department of Physics, SGM College Kurkheda, Maharashtra ,India
[2]Department of Physics, N. H. College, Bramhapuri, Maharashtra ,India
[3]Department of Physics, M.G. College, Armori, Maharashtra ,India
[4]Ex-Head Department Of Physics RTM Nagpur University, Nagpur, Maharashtra ,India

ABSTRACT

In the present work, $Sr_{4-x}Al_6MoO_{16}$:xEu^{3+}(x= 2,3,4 &5 %) red-emitting phosphors have been successfully synthesized by the combustion method and their photoluminescence characterization was performed. Photoluminescence spectra showed that the emission peaks at 593 ($^5D_0 \to {}^7F_1$) and 615 nm ($^5D_0 \to {}^7F_2$) for Eu^{3+} are observed after excitation at 270 nm (i.e. Mo–O charge transfer band). Intense red emission of Eu^{3+} in $Sr_{4-x}Al_6MoO_{16}$ host lattice show the occupation of a non-centrosymmetric site by the rare earth ions in the host lattice. The emission intensity of Eu^{3+} ions in the $Sr_{4-x}Al_6MoO_{16}$ host largely enhanced with the concentration increasing of activator (Eu^{3+}). Intense characteristic emissions show no concentration quenching up to 3 mol% concentration of rare earth ion and the emission intensity reached the maximum at x=4%. Among these phosphors, $Sr_{4-x}Al_6MoO_{16}$:xEu^{3+} synthesized at 750℃ exhibits the strongest red emission and appropriate CIE chromaticity coordinates (x=0.637, y=0.359) close to the NTSC standard value. It is shown that $Sr_{4-x}Al_6MoO_{16}$:xEu^{3+} phosphors are demonstrating their potential suitability for application in solid state lighting.
Keywords: Phosphors; Combustion Method; $Sr_{4-x}Al_6MoO_{16}$:xEu^{3+} ;Luminescence

I. INTRODUCTION

With the emerging global energy disaster and challenge caused by climate change, rare earth luminescent materials play a more and more important role in solid-state-lighting due to their exclusive electronic, optical, and chemical properties resulted from the 4f shell of the rare earth ions and are extensively applied to high performance luminescence devices, catalysts and other functional materials, etc [1]. In recent years, the light-emitting devices and optical phosphors of white light-emitting diodes (W-LEDs) have been paid much attention because of its wide applications as well as its advantages, for example, high color rendering index (CRI), long life time, high luminescence efficiency, low power consumption, and environment friendly [2–5]. Rare earth doped solid-state molybdates and tungstates exhibit outstanding chemical stability and long wavelength emission. Among these, rare earth doped scheelite-type ($CaWO4$) molybdates and tungstates have a large potential for use in WLEDs.[6–10] Recently a new application field has emerged for these materials as thermographic phosphors, due to their capacity to accurately visualize temperature gradients with high spatial resolution.[11] Due to charge transfer from oxygen to metal, tungstate and molybdate phosphors have intense, broad absorption bands in the near-UV region. Some scheelite-type compounds, such as $PbMoO_4$, $KGd(WO_4)_2$, $NaBi(WO_4)_2$ and MWO_4 (M = Pb, Cd, Ca) are well-known and used, while other $MLn(BO_4)_2$ (M = Li, Na, K, Ag; Ln = lanthanides, B = W, Mo) materials with Eu^{3+} cations are frequently suggested as red phosphors for WLEDs. For example, $NaEu(WO_4)_2$ and $KGd_{0.75}Eu_{0.25}(MoO_4)_2$ show strong, saturated red emission.[12-13]

To date, many methods have been used for the preparation of phosphor, such as hydrothermal method

[14] , solid-state reaction [15], combustion method [16], spray pyrolysis method [17], sol–gel [18,19], chemical vapor deposition (CVD) [20] , etc. The most widely used synthesis method is the solid-state method, and many important luminescent materials have been prepared by solid-state process. Liu and Su [21] have prepared $Ca_8[Al_{12}O_{24}](WO_4)_2{:}Tb^{3+}$ phosphor by the high-temperature solid-state method in which prolonged annealing at 1200 ^oC for 6 h and then at 1380 ^oC for 17 h. However, to the best of our knowledge, the combustion synthesis of $Sr_{4-x}Al_6MoO_{16}{:}xEu^{3+}$ ($SAMO{:}Eu^{3+}$) has not been reported. Combustion method compared with the high-temperature solid-state reaction has some advantages such as the improvement in processing time, the energy saving and the fine particle nature of the combustion products [22]. The same technique is now well established for borates [23], aluminates [24, 25] and tungstates [26] preparation, but in this work, we utilized combustion methods for the synthesis of rare earth Eu^{3+} activated $Sr_{4-x}Al_6MoO_{16}$ phosphors and their photoluminescence (PL) properties were studied.

II. EXPERIMENTAL

All chemicals were analytic grade and directly used without further purification. Distilled water was used throughout. The synthetic process of the products $Sr_{4-x}Al_6MoO_{16}{:}xEu^{3+}$ (x= 2,3,4 & 5%)) can be divided into two stages. Firstly, solution **A** was prepared by dissolving Eu_2O_3 with concentrated nitric acid, the excess HNO_3 was removed by further evaporation. Solution B was obtained by dissolving $Sr(NO_3)_2$, $Al(NO_3)_3.9H_2O$ and $(NH_4)_6Mo_7O_{24} .24H_2O$ in distilled water. Then the two solutions were fully mixed to get a transparent solution. A weighted amount of Urea (NH_2-CO-NH_2) were dissolved in the transparent solution as fuel and accelerator, respectively. The mixture gel was obtained after stirring and heating at 70 ^oC for 2h. The sticky gel was introduced into a preheated muffle furnace at a temperature of 750 ^oC and maintained for 5min. An auto combustion process took place, and a white precursor was obtained.

III. RESULTS AND DISCUSSION

3.1 PL Characteristics of $Sr_{4-x}Al_6MoO_{24}{:}xEu^{3+}$ Phosphor:
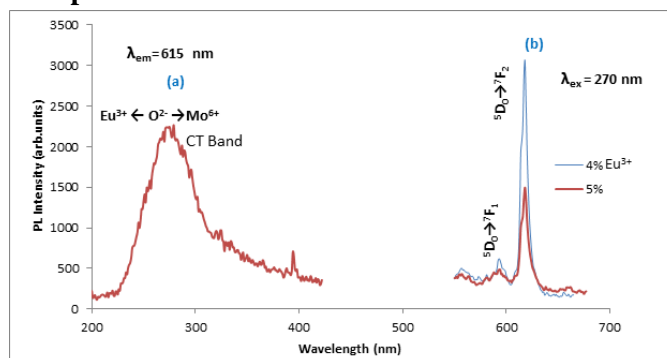
Figure 1. Excitation (left) and emission (right) spectra of $Sr_{4-x}Al_6MoO_{16}{:}xEu^{3+}$ (x=4% & 5%) phosphor.

Figure 1(a). shows the excitation spectra of $Sr_{4-x}Al_6MoO_{24}{:}xEu^{3+}$ sample monitoring the emission wavelength at 615 nm. The broad peak at 220–350 nm and sharp peaks with low intensity between 350–450 nm are observed. The Broad band peaking at 270 which correspond to the transition of charge transfer (CT) type from filled 2p orbitals of O^{2-} to empty 5d orbitals of Mo^{6+} within $(MoO_4)_2$ complex. The excitation spectra of red emission (615 nm) consists of a broad band in the vicinity of 250–350 nm having maximum at 270 nm and number of sharp peaks centered at 362, 377, 384, 395 and 410nm. The broad band attributes to interweaved CT band of $Mo^{6+} – O^{2-}$ and $Eu^{3+} –O^{2-}$ [27] .

The CTB is related to the stability of the electron of the surrounding O^{2-} ion i.e., the CT transition is sensitive to a ligand environment (the bonding energy between the central ion and the ligand ions). The fact that it occurs in the solid state (ionic oxides) is explained by the strong potential field at the anion (O^{2-}) sites due to the surrounding ions. If this potential increases, the energy required transferring an electron from the O^{2-} ion to the cation (Eu^{3+}) also increases, and the CTB moves to higher energy side.[28-30] In case of nanoscale samples, especially very tiny ones, the Eu-O distance is long, indicating that the Eu-O bonds become weaker, less covalent and high ionicity, which weakens the binding energy of an electron to O^{2-} . Therefore, the electron needs less energy to transfer from O^{2-} to Eu^{3+}, resulting in the CTB placed in the lower energy region. On the other hand, as particle size increases the surface to the volume ratio decreases and Eu-O distance is short. As a result, it requires more energy to remove an electron

from an O^{2-} ion; therefore, the CTB shifted towards higher energy. These results are also consistent with the Hoefdraad's study on the CTB of Eu^{3+} in oxides, where he concluded that the CTB band position of Eu-doped oxide depends on the bond length of Eu-O and the coordination environment around Eu^{3+} [31]. The sharp excitation peaks due to intra-configurationally f–f transitions were reported at 255 nm ($^8S_{7/2} \rightarrow {}^6D_{9/2}$), 275 nm ($^8S_{7/2} \rightarrow {}^6I_{11/2}$) and 277 nm ($^8S_{7/2} \rightarrow {}^6I_{9/2}$).[9] While peaks at ~362, 376, 382, 396, 412, 466 and 532 nm are assigned to $^7F_0 \rightarrow {}^5D_4$, $^7F_0 \rightarrow {}^5G_3$, $^7F_0 \rightarrow {}^5G_4$, $^7F_0 \rightarrow {}^5L_6$, $^7F_0 \rightarrow {}^5D_3$, $^7F_0 \rightarrow 5D_2$ and $^7F_0 \rightarrow {}^5D_1$, respectively of intra-configurationally f–f transitions of Eu^{3+} ions.

Figure 1(b) shows the emission spectra of $Sr_{4-x}Al_6MoO_{24}:xEu^{3+}$ (x= 4 & 5 mol%) phosphor excited at 270 nm. Under the excitation of 270 nm the emission spectra show a broad band extending from violet to red region of visible spectrum and this broad band is attributed to CT transition within $(MoO_4)^{2-}$ complex and termed as annihilation of self-trapped exciton. From 500 to 750 nm in Figure 4, there are four groups of the characteristic emission lines of Eu^{3+} assigned to the transitions of $^5D_0-^7F_J$ (J=1–4). The emission peaks at around 591, 618, 652 and 702 nm correspond to the transitions of $^5D_0 \rightarrow {}^7F_1$, $^5D_0 \rightarrow {}^7F_2$, $^5D_0 \rightarrow {}^7F_3$ and $^5D_0 \rightarrow {}^7F_4$, respectively [32]. It is well known that $^5D_0 \rightarrow {}^7F_1$ and $^5D_0 \rightarrow 7F_3$ transitions are ascribed to magnetic dipole transitions, while $^5D_0 \rightarrow {}^7F_2$ and $^5D_0 \rightarrow 7F_4$ transitions are due to electric dipole transitions. The strongest emission at 615 nm originating from the electric dipole transition of $^5D_0-^7F_2$ which is hypersensitive to the local environment [33]. The intensity of the transition between different J levels of Eu^{3+} depends upon the symmetry of the local environment of the activators. The main emission comes from the electric dipole transition of $^5D_0 \rightarrow {}^7F_2$ when Eu^{3+} ions occupy the sites without inversion centers. While Eu^{3+} ions have inversion symmetry sites, the magnetic dipole transition of $^5D_0 \rightarrow {}^7F_1$ will become stronger. From our results, the emission of Eu^{3+}-doped $Sr_{4-x}Al_6MoO_{16}$ is a typical emission of Eu^{3+} occupying the sites without inversion centers field in which the main emission comes from the electric dipole transition of $^5D_0 \rightarrow {}^7F_2$ for Eu^{3+} ion.

3.2 The effect of Eu^{3+} concentration on the red emission of $Sr_{4-x}Al_6MoO_{16}:xEu^{3+}$ phosphors
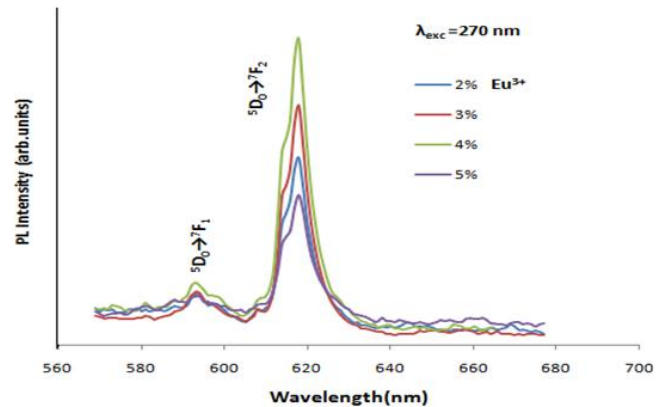
Figure 2. Emissions spectra of $Sr_{4-x}Al_6MoO_{16}:xEu^{3+}$ (x=2, 3, 4 and 5 %) phosphor
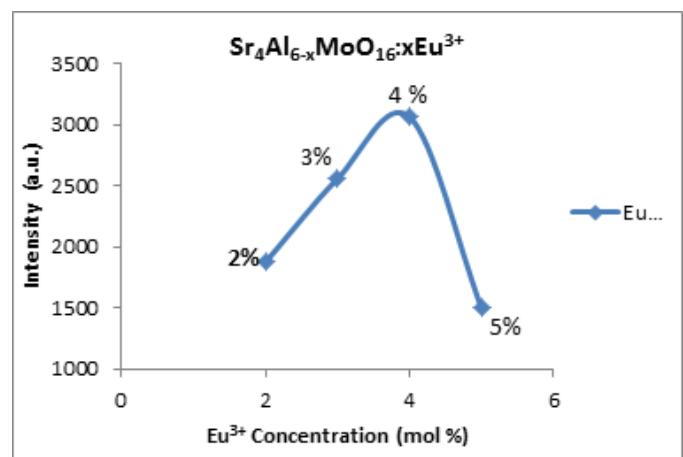
Figure 3. Luminescence intensity of $Sr_{4-x}Al_6MoO_{16}:xEu^{3+}$ as function of Eu^{3+} concentration.

The luminescence intensity of phosphor is strongly influenced by the activator concentration. It is well known that a low doping of Eu^{3+} in a compound leads to a weak luminescence, while heavy doping causes the "concentration quenching" of the luminescence. In order to obtain the best doping concentration of Eu^{3+}, a series of $Sr_{4-x}Al_6MoO_{16}:xEu^{3+}$ (x= 2,3,4,& 5%) samples have been synthesized. Figure 2 shows the emission spectra of Eu^{3+} doping aluminum molybdate measured at room temperature as a function of the Eu^{3+} concentration. The optimal doping concentration had to be confirmed to obtain the maximum luminescent intensity. As shown in Figure 3, all of the emission spectra exhibit the similar profile with different relative intensities, the luminescent intensity increases with increasing Eu^{3+} concentration (x value), and the concentration quenching can be found at x=4% . This quenching process is often attributable to the fact that the energy of electron in an excited state will be transmitted to the quenching center more easily

when the concentration of Eu^{3+} has reached a certain value [34–37]. What is more as the concentration of Eu^{3+} ions increases, a slight shift of the CT band maximum towards longer wavelength can be observed. It can be related to reduction of the average crystallite size with increasing concentration of Eu^{3+} ions doped into the host lattice. According to Ref. [38], the shift of CT band also depends on the distance between Eu^{3+}–O^{2-} ions and bond covalency. A shorter distance results in higher covalency and thereby there is a smaller difference between electronegativity of the above ions, thus the CT band shifts to higher wavelengths. This dependence is called the nephelauxetic effect.
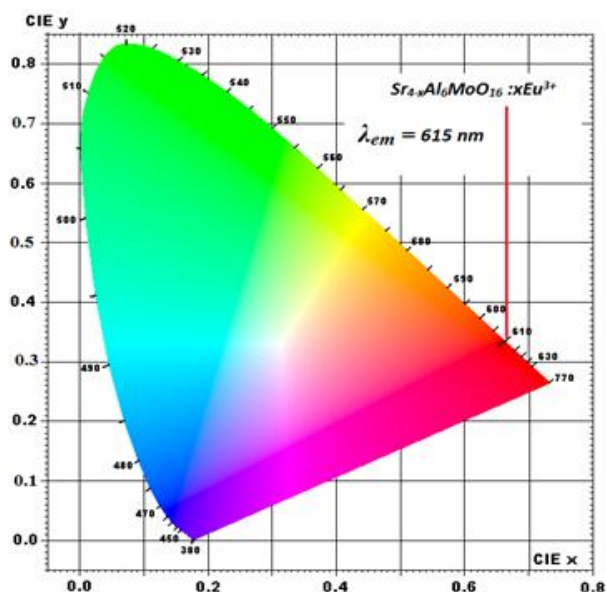
Figure 4. CIE Diagram Indicating The Color Coordinates From Emission Spectrum (Under 270 nm Excitation) Of $Sr_{4-x} Al_6MoO_{16} : xEu^{3+}$ Phosphors And The NTSC Standard value.

Figure 4. Shows the CIE diagram indicating the color coordinates from emission spectrum (under 270 nm excitation) of $Sr_{4-x} Al_6MoO_{16}: xEu^{3+}$ phosphors and the NTSC standard value. It can be clearly seen that the color coordinates of $Sr_{4-x}Al_6MoO_{16}:xEu^{3+}$ phosphor is very close to the NTSC standard value. Hence $Sr_{4-x}Al_6MoO_{16}:xEu^{3+}$ phosphor is considered as promising red phosphor for application in solid state lighting.

IV. CONCLUSION

$Sr_{4-x}Al_6MoO_{16}:xEu^{3+}$ phosphors were successfully synthesized by combustion method. When excited by UV light (270 nm), all samples of Eu^{3+}-doped $Sr_{4-x}Al_6MoO_{16}$ show red emission with the maximum intensity at 615 nm assigned to the $^5D_0{\rightarrow}^7F_2$ electric dipole transition of Eu^{3+} ion, and it is demonstrated that Eu^{3+} prefers to occupy the sites without inversion centers field. Therefore $Sr_{4-x} Al_6MoO_{16}:xEu^{3+}$ is a good red phosphor for White LED and appropriate CIE chromaticity coordinates (x=0.637, y=0.359) close to the NTSC standard values (x=0.66, y=0.33), and it may be served as near UV InGaN chip-based red-emitting LED phosphors. The results show that the $Sr_{4-x}Al_6MoO_{16}:xEu^{3+}$ phosphors have promising applications in displays, fluorescence probing and solid state- lighting in the future.

V. REFERENCES

[1]. W.O. Gordon, J.A. Carter, B.M. Tissue, J. Lumin. 108 (2004) 339.

[2]. X.M. Zhang, W.L. Li, L. Shi, X.B. Qiao, H.J. Seo, Appl. Phys. B., 99, 279.

[3]. K. Shioi, N. Hirosaki, R.J. Xie, T. Takeda, Y.Q. Li, J. Alloy. Compd. 504 (2010) 579.

[4]. D.Q. Chen, Y.L. Yu, P. Huang, H. Lin, Z.F. Shan, Phys. Chem. Chem. Phys. 12 (2010) 7775.

[5]. X. Zhang, J. Zhang, R. Wang, M. Gong, J. Am. Ceram. Soc. 93 (2010) 1368.

[6]. Kim, T.; Kang, S. Potential red phosphor for UV-white LED device. J. Lumin. 2007, 122−123, 964−966.

[7]. Hwang, K.-S.; Jeon, Y.-S.; Hwangbo, S.; Kim, J.-T. Opt. Appl. 2009, 39, 375−383.

[8]. Ya n , B . ; Wu , J . - H . Mater. Chem. Phys. 2009, 116, 67− 71.

[9]. Haque, Md. M.; Lee, H.-I.; Kim, D.-K. J. Alloys Compd. 2009, 481, 792−796.

[10]. Guo, C.; Gao, F.; Xu, Y.; Liang, L.; Shi, F. G.; Yan, B. J. Phys. D: Appl. Phys. 2009, 42, 095407.

[11]. Meert, K. W.; Morozov, V. A.; Abakumov, A. M.; Hadermann, J.; Poelman, D.; Smet, P. F. Opt. Express 2014, 22, A961−A972.

[12]. Shao, Q.; Li, H.; Wu, K.; Dong, Y.; Jiang, J. J. Lumin. 2009, 129, 879−883.

[13]. Yi, L.; Zhou, L.; Wang, Z.; Sun, J.; Gong, F.; Wan, W.; Wang, W. Curr. Appl. Phys. 2010, 10, 208−213.

[14]. L. Bokatial, S. Rai, J. Opt. 41 (2012) 94.

[15]. G.Y. Dong, H.X. Ma, Y.F. Liu, Z.P. Yang, Q.B. Liu, Opt. Commun. 295 (2013) 129.

[16]. N. Suriyamurthy, B.S. Panigrahi, B. Venkatraman, V. Natarajan, J. Opt. 41 (2012) 48.

[17]. G.R. Hu, X.R. Deng, Z.D. Peng, Y.B. Cao, K. Du, J. Alloy. Compd. 452 (2008) 462.

[18]. C. Mansuy, J.M. Nedelec, C. Dujardin, R. Mahiou, Opt. Mater. 29 (2007) 697.

[19]. Y.Q. Zhai, Z.H. Yao, S.W. Ding, M.D. Qiu, J. Zhai, Mater. Lett., 57, 2901.

[20]. Y.H. Li, J.H. Zhang, Q.Q. Xiao, R.J. Zeng, Mater. Lett. 62 (2008) 3787.

[21]. S.L. Liu, Q. Su, Chin. J. Chem. 22 (2004) 437.

[22]. X. Li, Z.P. Yang, L. Guan, Q.G. Guo, C. Liu, P.L. Li, J. Alloy. Compd. 464 (2008) 565.

[23]. G.F. Li, Q.X. Cao, Z.M. Li, Y.X. Huang, H.Q. Jiang, J. Rare Earths 28 (2010) 709.

[24]. T.Y. Peng, H.P. Yang, X.L. Pu, B. Hu, Z.C. Jiang, C.H. Yan, Mater. Lett. 58 (2004) 352.

[25]. S.K. Shi, J.Y. Wang, J. Alloy. Compd. 327 (2001) 82.

[26]. X.H. Qian, X.P. Pu, D.F. Zhang, L. Li, M.J. Li, S.T. Wu, J. Lumin. 131 (2011) 1692.

[27]. S.K. Shi, J. Gao, J. Zhou, Opt. Mater. 30 (2008) 1616.

[28]. G. Blasse, J. Chem. Phys. 1966, 45, 2356.

[29]. T. Igarashi, M. Ihara, T. Kusunoki, K. Ohno, T. Isobe, M. Senna, Appl. Phys. Lett. 2000, 76, 1549.

[30]. Z. Qi, M. Liu, Y. Chen, G. Zhang, M. Xu, C. Shi, W. Zhang, M. Yin, Y. Xie, J. Phys. Chem. C 2007, 111, 1945.

[31]. H. E. Hoefdraad, F. M. A. Stegers, G. Blasse, Chem. Phys. Lett. 1975, 32, 216.

[32]. Y. Wang, T. Endo, L. He, C. Wu, J. Cryst. Growth 268 (2004) 568.

[33]. L. Yang, L.Q. Zhou, Y. Huang, Z.W. Tang, Mater. Res. Bull. 46 (2011) 239.

[34]. D. Wang, Q.R. Yin, Y.X. Li, M.Q. Wang, J. Lumin. 97 (2002) 1.

[35]. L. Jiang, C.K. Chang, D.L. Mao, C.L. Feng, Mater. Sci. Eng. B 103 (2003) 271.

[36]. X.M. Zhang, H.J. Seo, J. Alloy. Compd. 503 (2010) L14.

[37]. J.L. Huang, L.Y. Zhou, Z.P. Zhao, F.Z. Gong, J.P. Han, R.F. Wang, J. Rare Earths 28 (2010) 356.

[38]. A. Szczeszak, K. Kubasiewicz, S. Lis, Opt. Mater. 35 (2013) 1297.